DYNAMIC CONTROL STRATEGIES FOR A SOLAR-ORC SYSTEM USING FIRST-LAW DYNAMIC AND DATA-DRIVEN MACHINE LEARNING MODELS

Zheng Liu[1], Alessandro Romagnoli[1,*], Paul Sapin[2], Christos Markides[2], Matthias Mersch[2]

[1] *School of Mechanical and Aerospace Engineering, Nanyang Technological University, 639798, Singapore*

[2] *Clean Energy Processes (CEP) Laboratory, Department of Chemical Engineering, Imperial College London, South Kensington Campus, London SW7 2AZ, UK*

*Corresponding Author: a.romagnoli@ntu.edu.sg

ABSTRACT

In this study, we developed and assessed the potential of dynamic control strategies for a domestic scale 1-kW solar thermal power system based on a non-recuperated organic Rankine cycle (ORC) engine coupled to a solar energy system. Such solar-driven systems suffer from part-load performance deterioration due to diurnal and inter-seasonal fluctuations in solar irradiance and ambient temperature. Real-time control strategies for adjusting the operating parameters of these systems have shown great potential to optimise their transient response to time-varying conditions, thus allowing significant gains in the power output delivered by the system. Dynamic model predictive control strategies rely on the development of computationally efficient, fast-solving models. In contrast, traditional physics-based dynamic process models are often too complex to be used for real-time controls. Machine learning techniques (MLTs), especially deep learning artificial neural networks (ANN), have been applied successfully for controlling and optimising nonlinear dynamic systems. In this study, the solar system was controlled using a fuzzy logic controller with optimised decision parameters for maximum solar energy absorption. For the sake of obtaining the optimal ORC thermal efficiency at any instantaneous time, particularly during part-load operation, the first-law ORC model was first replaced by a fast-solving feedforward network model, which was then integrated with a multi-objective genetic algorithm, such that the optimal ORC operating parameters can be obtained. Despite the fact that the feedforward network model was trained using steady-state ORC performance data, it showed comparable results compared with the first-principle model in the dynamic context, with a mean absolute error of 3.3 percent for power prediction and 0.186 percentage points for efficiency prediction.

1 INTRODUCTION

Solar energy is a particularly promising energy resource due to its clean, abundance and sustainable benign nature. Photovoltaic (PV) (Aktas et al., 2018; Li and Qiu, 2016) and PV-thermal (PVT) (Herrando et al., 2018; Wang et al., 2019) technologies have gained significant attention in recent years as a means to create electricity from the sun's light, attributed to the fall in price of these technologies. The Organic Rankine Cycle (ORC) engine is one of these technologies being explored as an alternative to PV for the transformation of solar radiation into electrical energy. By combining ORC with thermal energy storage (TES) system, the integrated system can store solar heat (for example, as hot water) for domestic heat supplying and electrical load profile matching, giving it an advantage over solar-PV systems (Freeman et al., 2015).

The Organic Rankine Cycle (ORC) is a closed thermodynamic power cycle based on the Rankine cycle that can produce electricity in the range of a few kilowatts to ten megawatts. Instead of using water as the working fluid, ORC system employs organic fluids to efficiently generate electricity from low- and medium-temperature heat sources from 65 °C up to 400 °C (Petrollese and Cocco, 2019). In a solar-powered ORC, solar irradiation is utilised to heat and evaporate the ORC working fluid at high pressure, which is then expanded to create mechanical shaft work. This shaft work can be utilised directly as

mechanical work, such as driving a pump, or it can be used to generate energy via a generator. Freeman et al. (2017) examined several combinations of collectors and phase change materials (PCMs) to investigate thermal energy storage alternatives for a solar-ORC system, with findings indicating that a 400-500 L PCM storage tank was required in the UK to produce a 1 kW-scale power output. Ramos et al. (2018) optimised a solar-ORC system for home use, taking into account two different types of solar collectors and seven different organic working fluids. They reported that with R245fa as the working fluid and R1233zd as the working fluid, the net power output of a 60 m^2 solar collector array in south European locations (average irradiance 600 W/m2) was 460 W and 1700 W, respectively.

Solar-ORC suffers from part-load performance deterioration due to daily and inter-seasonal dynamic fluctuations in solar irradiance and ambient temperature. Model-based predictive control strategies can be used to mitigate these problems. It does, however, rely on the creation of computationally efficient, fast-solving models, whereas traditional physical-based models are usually too complex to be employed for real-time controls. Data-driven models, particularly deep learning artificial neural networks (ANN), have been recently demonstrated success in controlling and optimising nonlinear systems. Zhao et al. (2020) reviewed artificial intelligence applied in the design of ORC in the aspects of decision making, parameter optimisation and parameter prediction. Yang et al. (2018) used a feedforward ANN model to optimise an ORC system for waste heat recovery of a diesel engine. They found if the ANN is coupled with the genetic algorithm, prediction accuracy can be significantly improved. Palagi et al. (2019) compared three different ANN models, namely the Feedforward, Recurrent and Long Short Term Memory networks, in the prediction of the dynamics of a 20 kW ORC system. Although the Long Short Term Memory model shows the best performance with a mean error smaller than 5%, it is still challenging to be implemented in the solar-ORC architecture owing to the high uncertainty of the weather, which can be hardly predicted correctly based on historical data.

Imran et al. (2020) comprehensively reviewed the dynamic control method over the years. Quoilin et al. (2011) presented the dynamic modelling and control strategy of ORC to improve efficiency during part-load operation. Their simulation results show that a model predictive control strategy based on optimised evaporating temperature regulation, which makes use of a steady-state optimisation model of the system bracketing a wide range of working conditions, gave the best results. Li et al. (2018) studied the influence factor such as the thermal storage system (TES) capacity, solar fluctuation (period, amplitude, average solar) and evaporation temperature on the dynamic performance of solar-ORC system. They suggested TES capacity should be selected according to local solar fluctuations to improve system stability. Baccioli et al. (2017) simulated the dynamic performance of a small-scale solar power plant with compound parabolic collectors and ORC module for the year-long operation. They adopted a sliding-velocity control strategy, allowing the system to operate without any storage.

To the best of the authors' knowledge, no previous study in the literature has applied data-driven models to dynamically control solar-ORC plants. Further researches are needed in developing an effective control logic for maximising the solar energy absorption while taking into account numerous aspects such as diurnal and inter-seasonal fluctuations, as well as real-time changes in thermal storage capacity. In this study, we developed a small-scale solar-ORC system model, which is designed for households combined heat and power usage, focusing on the specific user group at the location of London. An optimised fuzzy logic control algorithm was used to maximise the solar energy absorbed by the collector. The first-principle ORC model is replaced by a data-driven machine learning model (feedforward neuron network), which is then integrated with a multi-objective genetic algorithm (GA) to estimate optimal system operating parameters in real-time.

2 SYSTEM AND MODELLING DESCRIPTION

The ORC system model was developed according to the actual setup of the ORC testing facility located at the Clean Energy Processes Laboratory of Imperial College London. A detailed discussion of the ORC test facility was described by Unamba et al. (2019). The performance of a non-recuperative 1-kWe ORC engine with a rotary vane pump, brazed-plate evaporator and condenser units, and a scroll expander was investigated experimentally. It is worth mentioning that the test facility does not include the solar system so that the solar system was modelled by referring to the technical datasheet or literature. The solar system uses Therminol VP-1 as the heat transfer fluid (HTF) to heat the Organic working

fluid (R245FA) via a plate evaporator. The high-temperature, high-pressure working fluid expands in the expander to generate power before being cooled by cooling water in the condenser. Condensed working fluid is then pumped to the evaporator, completing the cycle.

Although the schematic view shows a solar and ORC coupled system, as shown in Fig. 1(a) , they are physically decoupled and modelled in different software. The ORC system was modelled using the one-dimensional differential equations with the physics described by the conservation of mass, momentum, and energy. These equations are solved by a differential-algebraic system solver DASSL using Dymola software, which is a simulation environment for Modelica-based models. Small time steps are required to solve these system equations to prevent chattering concerns caused by dynamic boundary conditions (Quoilin et al., 2014). Optimal control algorithms are necessary for the best adaptation to ever-changing heat source conditions, such as adjusting the pump speed and expander speed in real-time. Depending on the number of design variables, an optimisation process is generally converged after thousands of iterations. The authors employ an Intel Core i7-11700 to simulate the first-law model, and one case/iteration comparable to the daily operation of ORC system takes 15–20 minutes of CPU time to complete. Thus, it is not computationally efficient to use solar system and ORC system coupled simulation methods for optimisation purposes. Researchers (Christidis et al., 2012; Pérez-Iribarren et al., 2020; Benalcazar 2021) used a mixed-integer programming framework to simulate CHP with various scale TES and optimised the capacity of the TES; however, this is out of the scope of this study.

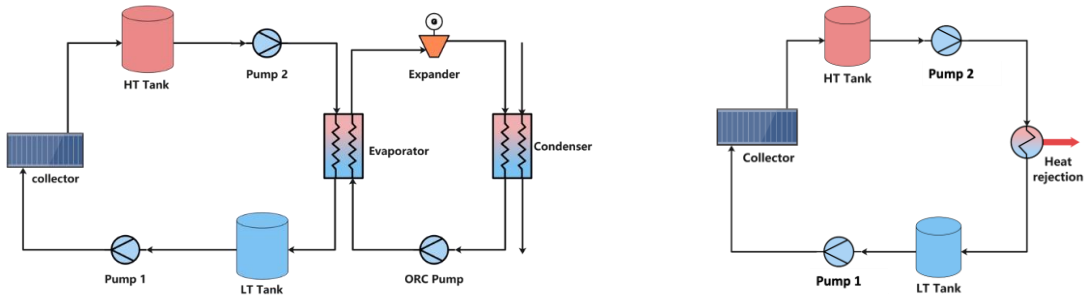

(a) (b)

Figure 1: (a) Schematic view of the solar-driven ORC system (b) solar system simulation method

The solar field was modelled in Simulink, utilising the Euler solver with a fixed time-step of 5 seconds. The solar system was physically decoupled with the ORC circuit, as shown in Fig. 1(b), but it was virtually connected to the ORC by using a heat rejection unit, which releases the thermal energy from the solar circuit as if it was used by the ORC system. The amount of rejected energy rates is calculated by dividing the demanded power by the ORC thermal efficiency, which is calculated using an ANN model that will be discussed in section.3.3. If the storage temperature goes below the intended level (120 °C) or the heat source flowrate falls below the threshold value of 0.5 kg/s, the quantity of heat rejection is set to zero, indicating that the ORC has been closed, prohibiting any inefficient operations.

In summary, the first-law ORC model served two functions. To begin, create a steady-state dataset that can be utilised to train a data-driven surrogate model later. Second, it can be used to assess the dynamic performance of a data-driven model. The solar model was used to test the efficacy of various control strategies under various seasonal conditions.

2.1 Solar collector

The solar field uses an evacuated flat-plate collector, designed by TVP Solar. The collector array is modelled as south-facing, with an inclination angle of 36° for the UK (Freeman et al., 2017). The heat absorbed by the collector is determined by the solar irradiance (G), total area of collector array (A_{sc}) and collector efficiency (η_{sc}), given by EQ. 1.

$$\dot{Q}_{sc} = GA_{sc}\eta_{sc} \quad (1)$$

The collector efficiency η_{sc} is calculated by EQ. 2, where T_a is the ambient temperature. η_0, a_1 and a_2 are correction parameters of the product, which are 0.76, 0.51, and 0.007 respectively.

$$\eta_{sc} = \eta_0 - \frac{a_1(T_{sc} - T_a)}{G} - \frac{a_2(T_{sc} - T_a)^2}{G} \quad (2)$$

2.2 Tanks

HT and LT tanks are developed by considering the conservation of mass and energy equations. The convective heat loss is adjusted to a level that the storage temperature (150 ℃) gradually drops to the ambient level after 8 hours if there is no flow moving into or out of the tank, as referred to Baccioli et al. (2017). The filling level (FL) of the tank is calculated by the EQ.3, where ρ is the density of the heat transfer fluid inside the tank; $M_{tk}$is the accumulated fluid mass inside the tank; V_{tk} is the volume of tank and is chose as a design parameter in this study. The actual value of V_{tk} will be determined from an optimisation study, as will be discussed in Section 3.2.3.

$$FL = \frac{M_{tk}}{\rho \cdot V_{tk}} \quad (3)$$

2.3 Evaporator and condenser

The evaporator uses a SWEP B12LX18 brazed-plate heat exchanger (HX) with an area of 0.45 m^2 and a nominal capacity of 10.63 kW. The condenser employs an Alfa Laval CB60-30H-F with a total heat-transfer area of 1.62 m^2 and a nominal capacity of 22 kW. Mersch (2019) evaluated the effects of different heat transfer correlations on the accuracy of model prediction using the same types of evaporator and condenser. They found Bogaert correlation (Bogaert and Böles, 1995) for Reynolds numbers below 1000 and the Chisholm correlation (Chisholm and Wanniarachchi, 1991) for higher Reynolds numbers gives the best model prediction for single-phase heat transfer. For two-phase heat transfer, they recommended using Cooper correlation (Cooper, 1984) to take the evaporate pool boiling effects into account and use Thonon correlation (Thonon and Bontemps, 2002) to calculate the condensation heat transfer.

Table 1: Design parameters of brazed-plate heat exchangers

Design parameters	Evaporator	Condenser
Num of plates	18	33
Pattern wavelength (m)	2.2e-2	3.2e-2
Pattern wave amplitude (m)	1.2e-3	1.6-e3
Pattern wave angle (degree)	60	35
Wall thickness (m)	1.8e-3	3.5e-3

However, due to the lack of detailed design information, such as the number of plates, wall thicknesses and pattern angle etc., this study used a fine-tuning procedure to estimate these parameters. This is a guess-and-verify process in which the HX design parameters are first approximated within a reasonable range and then matched to the intended heat transfer area. The fine-tuning process was performed for each HX for ten distinct operating points with varying heat source temperatures, mass flowrates, and work fluid mass flowrates. As listed in Table. 1, the HX design with the lowest mean differences relative to Mersch's(2019) results was decided.

2.4 Expander

The ORC uses a small-scale (~1 kW) scroll expander of which performance map was experimentally characterised by Lemort et al. (2012). The expander was designed with a swept volume of 22.4 cm^3/rev and a volume ratio of 2.85. The machine's highest isentropic efficiency is 71.03 percent, indicating that it has good volumetric performance. As per EQ.4, fifth-order (n=5) and second-order (n=2) polynomial are used to fit the experimentally measured efficiency and filling factor, resulting in R^2_{eff} 99.31 percent and R^2_{fill} 99.62 percent respectively. The expander's momentum inertia was ignored in this investigation since the expander's response time, which is around 8~11 seconds (Unamba et al., 2019), is insignificant compared to the response time of the solar-ORC with TES.

$$\sum_{i=0}^{n-1}\sum_{j=0}^{n-1} a_{ij}\cdot \ln(r_p)^i \cdot \ln(P_{in})^j + a_{n0}\cdot \ln(r_p)^n + a_{0n}\cdot \ln(P_{in})^n = f(r_p, P_{in}) \quad (4)$$

2.5 Pumps

The solar-ORC system has three pumps with a constant isentropic efficiency of 0.75 assumed for pump 1 and pump 2 due to lack of experimental data. This assumption can reasonably estimate the pump's power consumption as the pressure ratios of the first two pumps are small (less than 1.1), while the ORC pump should be explicitly modelled due to the larger pressure ratio encountered. The performance prediction of the ORC pump was based on the look-up of a spline surface fitted by the experimental data provided by Mersch (2019), as shown in Fig. 2.

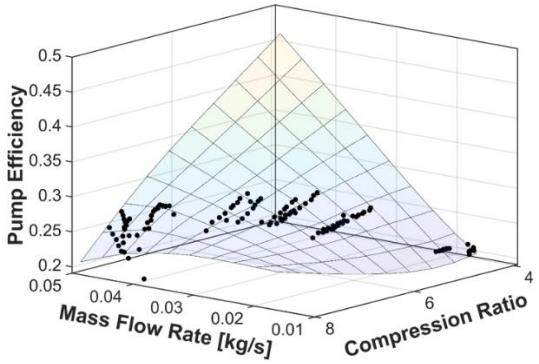

Figure 2: ORC pump map with spline surface fitted by the experiment data (Mersch, 2019)

2.6 Feasibility of ORC model

The ORC model's performance was assessed using experimental data provided by Imperial College London's Clean Energy Processes Laboratory (Unamba et al. 2019) under variable heat source temperatures and mass flowrates (16 g/s – 47 g/s), and constant heat sink temperature of 18 ℃ and water flowrates of 0.4 kg/s. As illustrated in Fig.3, the mean averaged percentage error is 3.2% at the heat source temperature is 120 $°C$. Although the error (8.2%) is higher at a higher heat source temperature (140 °C), the primary goal of this research is not to construct a high-fidelity first-law model, which has already been described in many publications. Instead, the objective of this research was to create a surrogate model of the first-law ORC model and assess the efficacy of employing the surrogate model for real-time control. As a result, the current model's accuracy indicates that it can reflect the overall trend of ORC performance under various operating conditions.

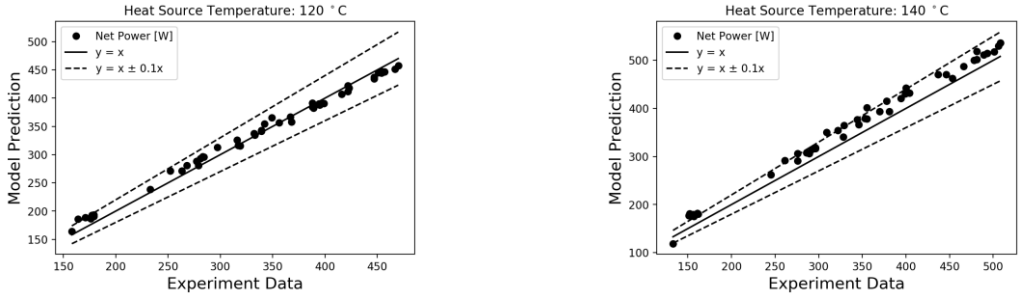

(a) (b)

Figure 3: Net power comparison between experimental data and model prediction on the basis of ORC system level at the heat source temperature of (a) 120 $°C$ and (b) 140 $°C$

3 SIMULATION AND CONTROL METHODOLOGY

3.1 Simulation boundary conditions

Diurnal and seasonal variations of solar irradiance were obtained from an open-source python package *pvlib* (Holmgren et al., 2018), which provides a set of functions and classes for simulating the performance of photovoltaic energy systems. As shown in Fig. 4(a), direct normal irradiation profiles

were retrieved for typical days in summer, winter and Autumn in London, which are mid of July, January and October. For simplicity, the weather conditions of Spring assumed the same as Autumn. The acquired direct normal irradiance profiles were rectified by taking into account the solar incidence angle on the tilted collector plane, and then fluctuating noises were introduced to capture the dynamics caused by cloudy weather. Diurnal and seasonal domestic electricity-load profiles for the UK (UK Energy Research Centre, 1997) are shown in Fig. 4(b), typically showing a characteristic peak in consumption in the evening occurring between 18:30 and 19:30. In the winter, the largest power usage was seen, along with the lowest irradiance and temperature. In order to meet the higher power usage in the winter, the solar collector would need a larger panel area than in the summer.

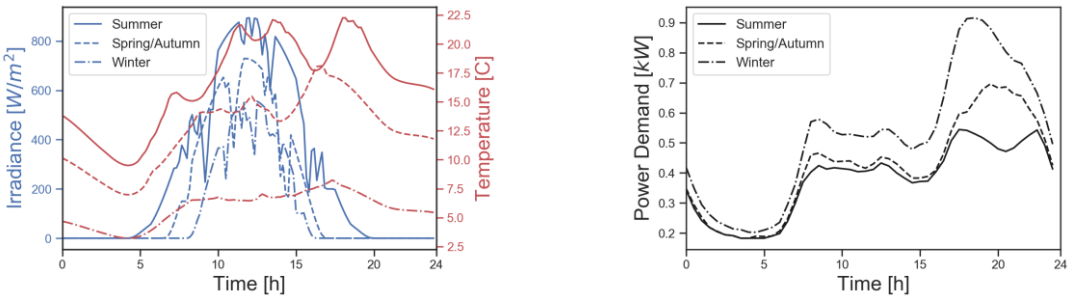

(a) (b)

Figure 4: (a) Diurnal and seasonal variations of solar irradiance and ambient temperature (b) UK average household electricity consumption profiles (UK Energy Research Centre, 1997)

3.2 Solar field dynamic control method

The objective is to obtain a control solution that can optimise the flowrates discharged by pump 1 and pump 2 such that the solar system can maximise the use of solar energy. The decision on the pump flow rate is influenced by various input conditions, i.e. the solar irradiance, filling level of tank and storage temperature, and these input conditions can also affect each other, resulting in high model nonlinearity. Safety precautions must be taken, such as not overcharging and emptying the tanks.

3.2.1 Pump 1 control method: The solar field's control logic should be built to suit the safety system's requirements while also allowing the solar field to supply sufficient energy to the ORC system. For this reason, fuzzy control algorithm was used to determine pump 1 flow rate. The fuzzy logic is a multivalued logical system that provides the value of an unknown output by attaching the degree of known input of the system. The fuzzy logic method divides inputs and outputs into linguistic levels based on their values, which are known as membership functions, and then calculates the degree of truth for each level. Fuzzy logic controller uses fewer resources and saves substantial computation time; therefore, it can be used for real-time control purposes.

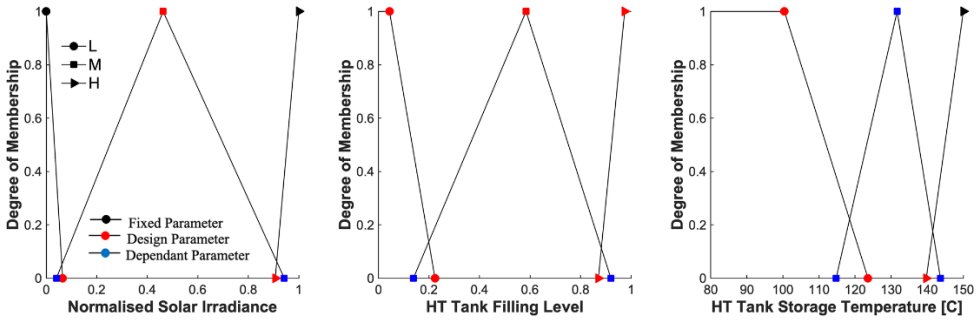

Figure 5: Membership functions of fuzzy logic input variables

As shown in Fig. 5, the linguistic levels assigned to three input variables, “Normalised solar irradiance”, “HT-Tank filling level” and “HT-Tank storage temperature” are L: Low; M: Medium and H: High. The y-axis is called the degree of membership, in which a higher value means the case has a higher possibility of belonging to the corresponding level. As shown in Fig. 6, the output variable was classified into five linguistic levels with additional VL (very low) and VH (very high) levels.

Once the membership functions of the input and output variables have been specified, the next stage is to define the rules and create logical linkages between the model inputs and outputs. As listed in Table. 2, nine rules have been defined. It is worth mentioning that the first two rules ensure a safe operation of the system, stating that if the filling level is low, the flow rate of pump 1 must be set to very high, preventing the use-up of fluid inside the tank and vice versa.

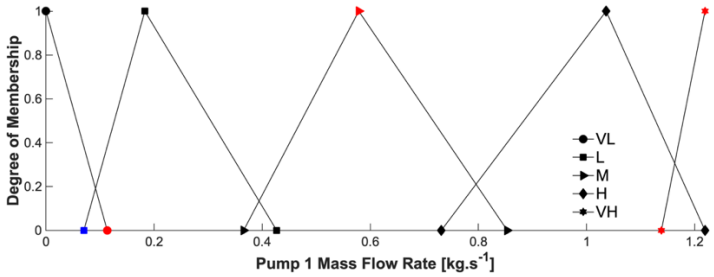

Figure 6: Membership functions of fuzzy logic output variables

Table 2: Decision matrix of the fuzzy logic controller used for pump 1 flowrate control

Rule Num	Irradiance	Filling Level	HT Tank Temperature	Pump 1 Flowrate
1	any	L	any	VH
2	any	H	any	VL
3	L	M	any	VL
4	M	M	L	L
5	M	M	M	M
6	M	M	H	H
7	H	M	L	M
8	H	M	M	H
9	H	M	H	H

VL: Very low; L: Low; M: Medium; H: High; VH: Very High

The last and most important step is to decide the range for each linguistic level and define the location of the highest possibility. This process was conventionally established based on the engineer's experiences and knowledge. This study employs GA for this decision making. As highlighted in Fig. 5 and Fig. 6, a red dot means it is a design variable to be optimised. A blue dot means it is a dependent variable and its location is influenced by the nearby design variable. The relative distance between the design variables and adjacent dependent variables is controlled by introducing additional design parameters. A black dot means that point is fixed through the study. Note that each point has one degree of freedom and can move along the x-axis only.

3.2.2 Pump2 control method: pump 2 controls the amount of heat flows going through the evaporator, thus having a direct influence on the ORC performance. Pump 2's control logic states that if the HT-storage Tank's temperature is less than the minimum required temperature, in this case 120 °C, pump 2 produces the same amount of flowrates as pump1, allowing the storage temperature to rise as the flow recirculates; otherwise, the flow rates of pump 2 refer to a 3rd order polynomial as per EQ. 5. This equation says that when the fill level of LT-tank is low (0<FL<0.2), pump2 increases its flow rate, avoiding the use up of the tank's oil and vice versa when the fill level is high (0.8<FL<1). Pump 2 maintains a relatively stable flow rate while the LT-tank is at a medium fill level (0.3<FL<0.7), allowing for a smooth ORC operation. Pump 2's nominal flow rate is close to 0.6 kg/s, which is expected to produce higher thermal efficiency based performance map.

$$\dot{m}_{pump2} = -3.57FL^3 + 4.92FL^2 - 2.35FL + 1 \quad (5)$$

3.2.3 Optimisation of the controller in the solar field: the solar system has 15 different parameters that define the fuzzy logic controller. Two new parameters were added to the optimiser to limit the system to an acceptable scale: tank volume and solar collector area. A multi-objective Genetic Algorithm, namely NSGA-II optimiser, was used for maximising the ORC daily work output. The maximum HT-

tank storage temperature should not exceed 154 °C, as this would cause the ORC fluid to surpass the critical temperature T_{crit} of R245FA, resulting in a supercritical cycle with high operating pressure beyond the proposed facility's design scope, which is usually achieved using nonlinear constraints. However, it significantly raises the computing cost, as it necessitates an exploration process to find a feasible design option before starting the actual simulation. For this reason, we impose a design choice similar to the nonlinear constraint, with the second GA objective being to minimise differences between the maximum HT-tank temperature and the T_{crit} of R245FA. It also sets a safety margin ε of 4 K, resulting in a maximum storage temperature of less than 150 ℃. The optimiser sets the population size of 200 and the crossover fraction of 0.65. The tank volume is set with a lower bound of 200 L and an upper bound of 500 L, and the solar collector area is ranging from 15 m^2 and 70 m^2. The design limits of the fuzzy logic controller are not listed here as they are not intuitive.

Table 3: ORC simulation matrix

Parameter	**Values**
Expander speed, Hz	10+5k, k = 1,2,…7
Pump Flow Rate, g/s	15+5k, k = 1,2,…,10
Heat source temp, °C	120,130,140,150
Heat source flow rate, kg/s	0.4+0.1k, k = 1,2,…,7

3.3 ORC dynamic control method

ORC dynamic control is designed to maximise ORC thermal efficiency for the target power output under continuously changing heat source conditions. The first-law dynamic ORC model was used to investigate several steady-state operating points as shown in the simulation matrix of Table. 3. After the simulation completes, an extensive dataset is generated, including 4279 valid ORC results. Fig.7 shows an example of the ORC performance map under the heat source temperature of 120 °C and heat source mass flowrate of 1 kg/s. It has been discovered that the same power output may be achieved using various combinations of expander speeds and pump flow rates.

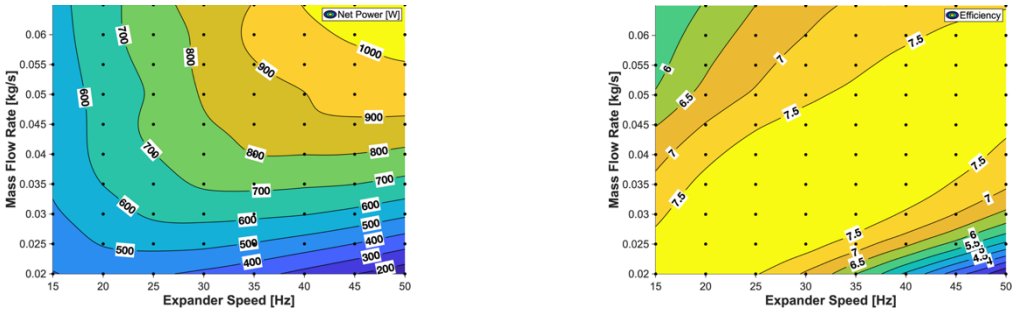

(a) (b)

Figure 7: ORC spline fitted (a) net power and (b) thermal efficiency contours as a function of expander speed and pump flowrate under heat source flow rate of 1kg/s and temperature of 120 °C

Feedforward neural networks were trained and represented as the surrogate model of the first-law model. The overall dataset was randomly split into 90% training dataset and 10% test dataset. Feedforward neural networks are the most basic ANN architecture, which is composed of neurons organised in layers forward connected to each other. The Keras platform was used to implement the feedforward neural networks. The input layer has four neurons corresponding to the four decision parameters as listed in Table. 3. Only one hidden layer that has 450 units was used as it is widely accepted that one hidden layer is enough for the resolution of almost any regression problem. The output layer has one unit, representing either the ORC thermal efficiency or the ORC net power. A dropout rate of 0.2 was used to prevent overfitting. The hidden layer uses ReLu as the activation function. Adam optimiser with a learning rate of 0.001 was used to minimise the mean square errors during the training process. The training phase has been performed using a batch size of 10.

Fig.8 shows the performance of the feedforward neural networks on the prediction of ORC thermal efficiency and ORC net power, and the respective R^2 are 0.98 and 0.99. The training and testing datasets

both have the same R^2 value, indicating that overfitting unlikely happens. The multi-objective GA was then integrated with the data-driven model to find the ideal expander speed and pump flow rate that can result in maximum thermal efficiency and supply the target power under a certain heat source temperature and flowrate condition.

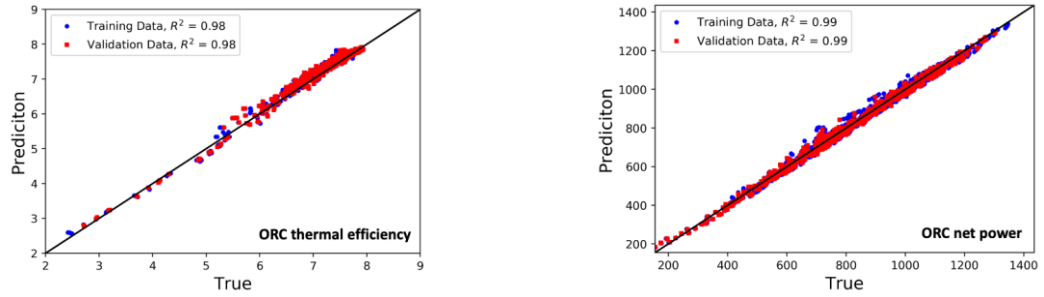

(a) (b)

Figure 8: Performance of feedforward neural networks on the prediction of (a) ORC thermal efficiency and (b) ORC net power

4 RESULTS AND DISCUSSION

4.1 Solar system optimisation results

The dynamic simulation of the solar system starts by assuming that both tanks reach the thermal equilibrium conditions and have an equivalent filling level of 0.5. Fig.9 shows the optimisation dataset under different seasonal conditions, with the optimal design highlighted by a red pentagram. The optimal designs were selected from the dataset by three steps (1) filtering the cases that have the maximum HT-tank temperature closer ($\pm$2℃) to the desired value (150 ℃); (2) the case that has the maximum daily work output was deemed as the optimal; (3) if there is no case found in the first step, the optimal design was selected based on the highest work output. The time-resolved operational profiles of optimised cases, such as instantaneous tank fill level, tank storage temperature, and mass flowrates of pumps, can be found in Appendix. A. As observed in Fig. 9(c), the maximum storage temperature is lower than 150 ℃ due to low irradiances during wintertime.

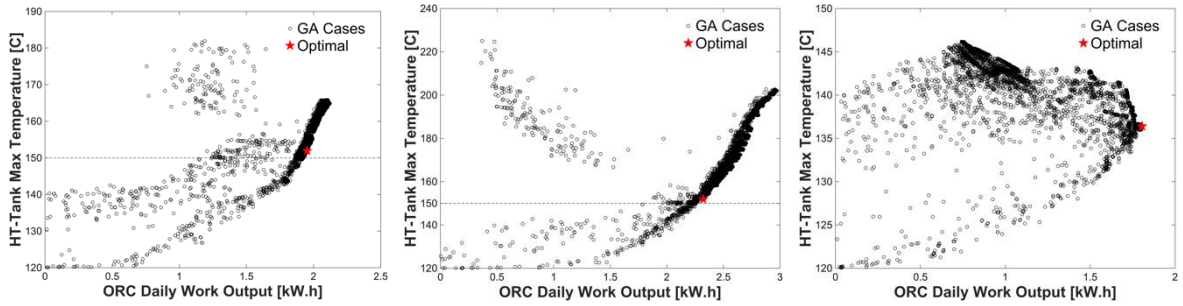

(a) (b) (c)

Figure 9: Solar system optimization results of (a) spring/autumn (b) summer (c) winter

Table 4: Summary of design and operational parameters of the optimal cases

	Spring/Autumn	**Summer**	**Winter**
Max Generations	48	24	25
Tank volume (L)	203	494	201
Collector area (m^2)	43.3	46.7	69.8
Daily work output (kWh)	1.95	2.32	1.75
Maximum tank temp (℃)	152	152	136.4
Start time	09:46	10:30	10:53
Stop time	14:18	16:21	14:12
Operation hours	4:32	5:51	3:19

Table. 4 summaries some key design and operational parameters of the optimal cases. The ORC produces the most significant daily work of 2.32 kWh during the summer, followed by 1.95 kWh in the spring/autumn, and 1.75 kWh in the winter. The tank capacities of spring/autumn/winter seasons tend to reach the lower bound of the design limits, as it is easier for a smaller sized tank to reach the ORC trigger temperature of 120 ℃ under low irradiance conditions. The summer case has the largest tank volume of all the cases, storing the most solar energy during the day and having the most prolonged working period of around 6 hours. According to the optimisation results, for the year-long operation in the United Kingdom, it is advised to install two 200 L tanks (no PCM) for both HT and LT tanks. During the spring/autumn and winter, one HT (LT) tank will be utilised instead of two.

The collector area in the spring/autumn cases is comparable to that in the summer cases. The collector area of the winter case almost reaches the upper bound of the design limits, attempting to maximise the energy absorption from the sun.

4.2 ORC optimisation results

A trained feedforward neuron network can forecast ORC power and efficiency by simply providing the input parameters, such as expander speed, pump flowrate, heat source temperature, and heat source mass flowrate. The instantaneous ORC boundary conditions, namely the HT-tank temperature and Pump 2 flowrate, are discretised into multiple quasi-steady points, as shown in Fig. 10. Therefore, the optimal expander speed and pump flowrate, which can result in the maximal thermal efficiency, can be obtained by integrating a multi-objective GA with the trained feedforward neuron network. Similarly, the differences between the required household electricity consumption and model-predicted value were served as another objective to be minimised. This process was repeated for each discretised operating point. With the current CPU power, the optimisation process converges in less than 30 seconds using the fast-solving data-driven model.

As Fig. 7 indicates, each optimisation process may produce a variety of feasible outputs of expander speeds and pump flowrates, all of which can result in the same thermal efficiency and power output, which may lead to system instabilities. To mitigate this, following the determination of the first set of outputs, the least distance criteria was used to pick the subsequent outputs. The distance refers to the differences in expander speeds and pump flowrates between consecutive cases, as per EQ.5. It's worth noting that these variables are first normalised, ensuring that they are all equally weighted concerning the distance.

$$D = \sqrt{\left(\frac{\omega_{i+1}}{\omega_{ref}} - \frac{\omega_i}{\omega_{ref}}\right)^2 + \left(\frac{\dot{m}_{i+1}}{\dot{m}_{ref}} - \frac{\dot{m}_i}{\dot{m}_{ref}}\right)^2} \tag{5}$$

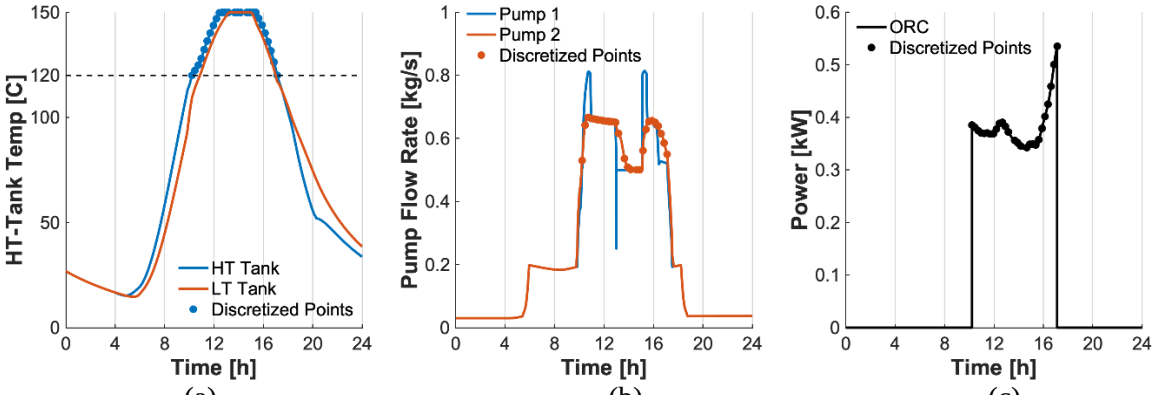

(a) (b) (c)

Figure 10: Instantaneous operational performance data of (a) storage temperature (b) pump flow rate (c) household power demand

Fig. 11 shows a diagram, which summarises the workflow of the proposed dynamic control method. The top-right figure shows the optimal ORC control solutions based on a series of steady-state optimisation of the discretised points. The final and most important step is to examine whether the

required power can be met whilst maintaining excellent ORC thermal efficiency. As shown in Fig.12 (a), both the data-driven model and the first-law model capture the trend of the target value using the control solutions. But it seems the model could not damp the secondary fluctuations, resulting in a non-smooth operating characteristic. It was found that the secondary fluctuations were mainly influenced by the pump flow rates. Therefore, it is anticipated that using data smoothing algorithms, such as moving average filter, can mitigate this situation. Nonetheless, the data-driven model demonstrates a good correlation with the first-law model, notably in terms of efficiency prediction, where the data-driven model accurately captures even minor traits. Given the fact that the optimisation of the dynamic data-driven ORC model was achieved in a quasi-steady manner, the small discrepancies between the first-law model and data-driven model imply the dynamics can be neglected when TES is included.

The mean absolute inaccuracy for the power estimate is 3.3 percent, while the mean absolute difference for the efficiency prediction is 0.186 percent. During the ORC's operation, a high averaged thermal efficiency of 7.5 percent was attained, demonstrating the effectiveness of data-driven methods in controlling nonlinear systems.

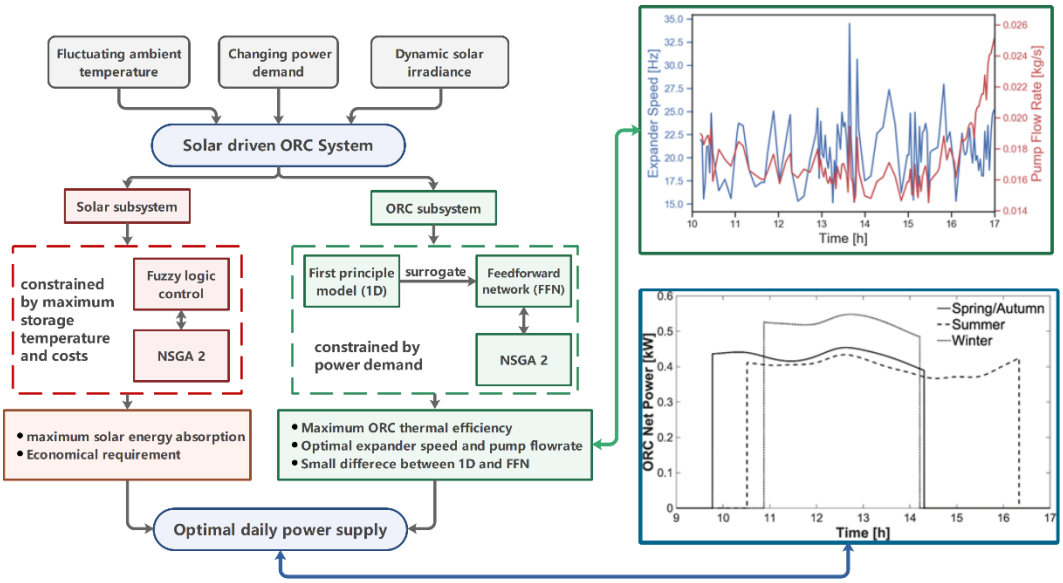

Figure 11: Summary of the proposed dynamic control method

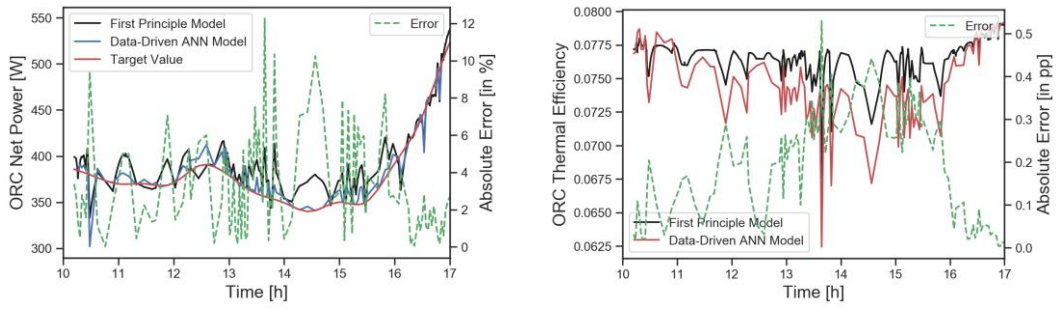

(a) (b)

Figure 12: Comparison between the first-law model and the data-driven model in terms of (a) net power output and (b) thermal efficiency

5 CONCLUSIONS

This study intends to develop a dynamic control strategy for a domestic scale 1-kW solar-driven ORC system in order to mitigate the inefficiency caused by daily and inter-seasonal solar energy changes. The solar-driven ORC system was decoupled into two subsystems and optimised separately. In the solar field, the flowrates released by pumps was managed with a fuzzy logic controller that used real-time

irradiance, tank storage temperature, and tank filling level as inputs. These inputs were classified into different linguistic levels, with the multi-object GA parameterising and optimising the ranges of each level. The dimensions of the solar collector and the tank were also factored into the optimisation process, keeping the system to a reasonable scale. The solar system can thereby maximise solar energy absorption in different seasons whilst keeping expenses relatively low.

The dataset obtained by the first-principle ORC model was used to train the feedforward neural network model, which showed good accuracy with an R^2 value of 0.98. The data-driven model was coupled with multi-objective GA to figure out the best expander speed and pump flowrate for maximum ORC thermal efficiency while also satisfying real-time household electricity consumption profiles. Despite the fact that the data-driven model was trained using a steady-state dataset, it displays minor discrepancies in dynamic simulations when compared to the first-principle model, with a mean absolute error of 3.3 percent for power prediction and 0.186 percentage points for efficiency prediction. This study suggests data-driven models coupled with quasi-steady optimisation methods can offer a promising solution for controlling the solar-driven ORC systems integrated with TES.

NOMENCLATURE

Notation		
ANN	artificial neural networks	
FL	filling factor	
HX	heat exchanger	
GA	Genetic algorithm	
ORC	Organic Rankine cycle	
TES	thermal energy storage	
HTC	heat transfer fluid	
HT	high temperature	
LT	low temperature	
MLTs	machine learning techniques	
A	area	m^2
a	Expander's fitting coefficients	
G	solar irradiance	W/m^2
T	temperature	K
M	mass	kg
V	volume	m^3
$\dot{Q}$	heat transfer rate	W
$\dot{m}$	mass flow rate	kg/s
c_p	specific heat capacity	J(kg. K)
P	pressure	Pa
ρ	density	kg/m^3
r_p	pressure ratio	
η	collector efficiency	
subscript		
sc	solar collector	
in	inlet	
out	ouetlet	
tk	tank	
a	Ambient	
eff	efficiency	
$crit$	critical	

REFERENCES

Aktas, A., Erhan, K., Özdemir, S. and Özdemir, E., 2018. Dynamic energy management for photovoltaic power system including hybrid energy storage in smart grid applications. Energy, 162, pp.72-82.

Baccioli, A., Antonelli, M. and Desideri, U., 2017. Dynamic modeling of a solar ORC with compound parabolic collectors: Annual production and comparison with steady-state simulation. Energy Conversion and Management, 148, pp.708-723.

Bogaert, R. and Böles, A., 1995. Global performance of a prototype brazed plate heat exchanger in a large Reynolds number range. EXPERIMENTAL HEAT TRANSFER An International Journal, 8(4), pp.293-311.

Benalcazar, P. 2021. Sizing and optimising the operation of thermal energy storage units in combined heat and power plants: An integrated modeling approach. Energy Conversion and Management, 114255.

Chisholm, D. and Wanniarachchi, A.S., 1991, March. Layout of plate heat exchangers. In ASME/JSME Thermal Engineering Proceedings (Vol. 4, pp. 433-438). ASME New York.

Christidis, A., Koch, C., Pottel, L., & Tsatsaronis, G. 2012. The contribution of heat storage to the profitable operation of combined heat and power plants in liberalised electricity markets. Energy, 41(1), 75-82.

Cooper, M.G., 1984. Heat flow rates in saturated nucleate pool boiling-a wide-ranging examination using reduced properties. In Advances in heat transfer (Vol. 16, pp. 157-239). Elsevier.

Freeman, J., Guarracino, I., Kalogirou, S.A. and Markides, C.N., 2017. A small-scale solar organic Rankine cycle combined heat and power system with integrated thermal energy storage. Applied thermal engineering, 127, pp.1543-1554.

Freeman, J., Hellgardt, K. and Markides, C.N., 2015. An assessment of solar-powered organic Rankine cycle systems for combined heating and power in UK domestic applications. Applied Energy, 138, pp.605-620.

Herrando, M., Ramos, A. and Zabalza, I., 2018. Cost competitiveness of a novel PVT-based solar combined heating and power system: Influence of economic parameters and financial incentives. Energy conversion and management, 166, pp.758-770.

Holmgren, W.F., Hansen, C.W. and Mikofski, M.A., 2018. pvlib python: A python package for modeling solar energy systems. Journal of Open Source Software, 3(29), p.884.

Imran, M., Pili, R., Usman, M., & Haglind, F. 2020. Dynamic modeling and control strategies of organic Rankine cycle systems: Methods and challenges. Applied Energy, 276, 115537.

Lemort, V., Declaye, S., Quoilin, S., 2012. Experimental characterisation of a hermetic scroll expander for use in a micro-scale Rankine cycle. Proceedings of the Institution of Mechanical Engineers, Part A: Journal of Power and Energy 226, 126–136.

Li, F.F. and Qiu, J., 2016. Multi-objective optimisation for integrated hydro–photovoltaic power system. Applied Energy, 167, pp.377-384.

Li, S., Ma, H. and Li, W., 2018. Dynamic performance analysis of solar organic Rankine cycle with thermal energy storage. Applied Thermal Engineering, 129, pp.155-164.

Mersch, M., 2019. Development of an experimentally validated Organic Rankine cycle model using computer-aided molecular design tools for the optimisation of waste-heat recovery systems. Clean Energy Processes Laboratory of Imperial College London. Master's Thesis.

Palagi, L., Pesyridis, A., Sciubba, E. and Tocci, L., 2019. Machine Learning for the prediction of the dynamic behavior of a small scale ORC system. Energy, 166, pp.72-82.

Petrollese, M. and Cocco, D., 2019. Robust optimisation for the preliminary design of solar organic Rankine cycle (ORC) systems. Energy Conversion and Management, 184, pp.338-349.

Pérez-Iribarren, E., González-Pino, I., Azkorra-Larrinaga, Z., & Gómez-Arriarán, I. 2020. Optimal design and operation of thermal energy storage systems in micro-cogeneration plants. Applied Energy, 265, 114769.

Quoilin, S., Aumann, R., Grill, A., Schuster, A., Lemort, V. and Spliethoff, H., 2011. Dynamic modeling and optimal control strategy of waste heat recovery Organic Rankine Cycles. Applied energy, 88(6), pp.2183-2190.

Quoilin, S., Bell, I., Desideri, A., Dewallef, P., Lemort, V., 2014. Methods to Increase the Robustness of Finite-Volume Flow Models in Thermodynamic Systems. Energies 7, 1621–1640. https://doi.org/10.3390/en7031621

Ramos, A., Chatzopoulou, M.A., Freeman, J. and Markides, C.N., 2018. Optimisation of a high-efficiency solar-driven organic Rankine cycle for applications in the built environment. Applied energy, 228, pp.755-765.

Thonon, B. and Bontemps, A., 2002. Condensation of pure and mixture of hydrocarbons in a compact heat exchanger: experiments and modelling. Heat transfer engineering, 23(6), pp.3-17.

UK Energy Research Centre, 1997, Electricity User Load Profiles by Profile Class, November. Available from: https://data.ukedc.rl.ac.uk/browse/edc/efficiency/residential/ LoadProfile

Unamba, C.K., Sapin, P., Li, X., Song, J., Wang, K., Shu, G., Tian, H. and Markides, C.N., 2019. Operational optimisation of a non-recuperative 1-kWe organic rankine cycle engine prototype. Applied Sciences, 9(15), p.3024.

Wang, K., Herrando, M., Pantaleo, A.M. and Markides, C.N., 2019. Technoeconomic assessments of hybrid photovoltaic-thermal vs. conventional solar-energy systems: Case studies in heat and power provision to sports centres. Applied Energy, 254, p.113657.

Yang, F., Cho, H., Zhang, H., Zhang, J. and Wu, Y., 2018. Artificial neural network (ANN) based prediction and optimisation of an organic Rankine cycle (ORC) for diesel engine waste heat recovery. Energy conversion and management, 164, pp.15-26.

Zhao, D., Deng, S., Zhao, L., Xu, W., Wang, W., Nie, X. and Chen, M., 2020. Overview on artificial intelligence in design of organic Rankine cycle. Energy and AI, p.100011.

APPENDIX

A. Transient performance of the solar system in different seasonal conditions

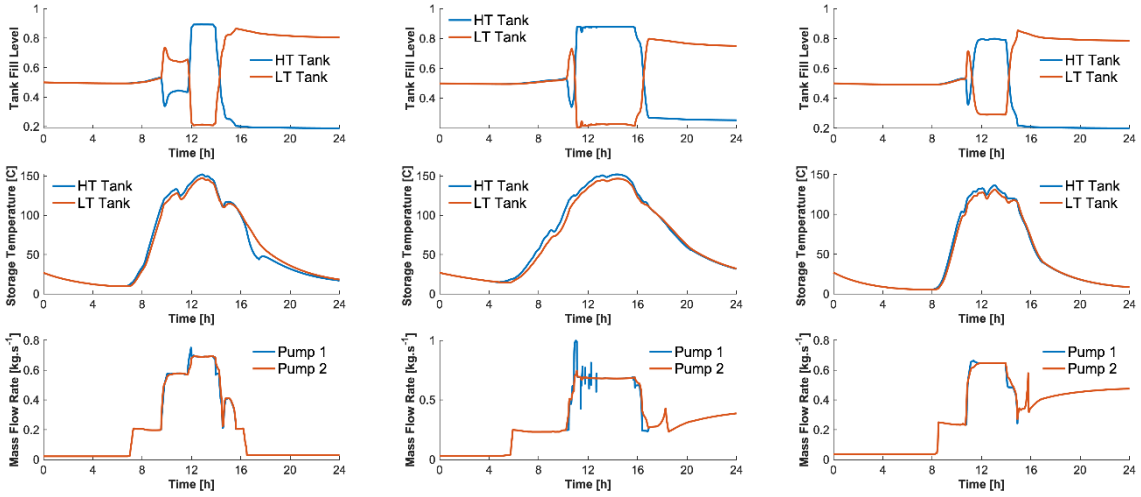

(a) (b) (c)

Figure A1: Solar system transient performance in (a) spring/autumn days (b) summer days (c) winter days